Antigen-Loaded Upconversion Nanoparticles for Dendritic Cell Stimulation, Tracking, and Vaccination in Dendritic Cell-Based Immunotherapy

Jian Xiang, Ligeng Xu,* Hua Gong, Wenwen Zhu, Chao Wang, Jun Xu, Liangzhu Feng, Liang Cheng, Rui Peng,* and Zhuang Liu*

Institute of Functional Nano & Soft Materials (FUNSOM), Collaborative Innovation Center of Suzhou Nano Science and Technology, Soochow University, Suzhou, Jiangsu 215123, China

ABSTRACT

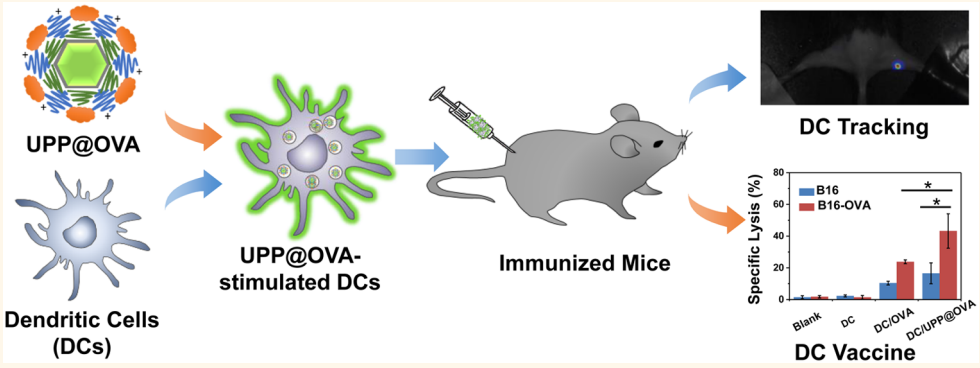

A dendritic cell (DC) vaccine, which is based on efficient antigen delivery into DCs and migration of antigen-pulsed DCs to draining lymph nodes after vaccination, is an effective strategy in initiating $CD8^+$ T cell immunity for immunotherapy. Herein, antigen-loaded upconversion nanoparticles (UCNPs) are used to label and stimulate DCs, which could be precisely tracked after being injected into animals and induce an antigen-specific immune response. It is discovered that a model antigen, ovalbumin (OVA), could be adsorbed on the surface of dual-polymer-coated UCNPs *via* electrostatic interaction, forming nanoparticle—antigen complexes, which are efficiently engulfed by DCs and induce DC maturation and cytokine release. Highly sensitive *in vivo* upconversion luminescence (UCL) imaging of nanoparticle-labeled DCs is successfully carried out, observing the homing of DCs to draining lymph nodes after injection. In addition, strong antigen-specific immune responses including enhanced T cell proliferation, interferon gamma (IFN-γ) production, and cytotoxic T lymphocyte (CTL)-mediated responses are induced by a nanoparticle-pulsed DC vaccine, which is promising for DC-based immunotherapy potentially against cancer.

KEYWORDS: DC vaccine · UCNP · sensitive tracking · immunotherapy

Dendritic cells (DCs), which are professional antigen-presenting cells in the mammalian immune system, play pivotal roles in the initiation and regulation of innate and adaptive immune responses.[1,2] The main function of DCs is processing antigens captured in peripheral tissues into peptides, presenting them on the cell surface to T lymphocytes, and subsequently initiating T cell or B cell immunity.[3] In recent years, DCs have been extensively exploited to develop DC-based immunotherapy to treat various puzzle diseases including HIV and cancer.[4−6] For example, *ex vivo*-generated DCs pulsed with tumor-associated antigens could be used as therapeutic vaccines against human cancers such as metastatic melanoma,[7] renal

* Address correspondence to zliu@suda.edu.cn, rpeng@suda.edu.cn, lgxu@suda.edu.cn.

Received for review April 3, 2015 and accepted May 30, 2015.

Published online May 31, 2015
10.1021/acsnano.5b02014

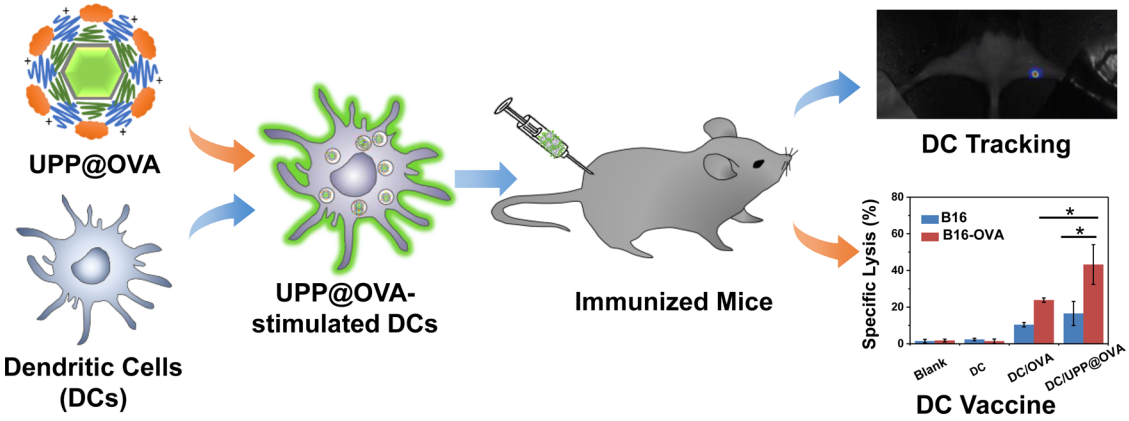

Scheme 1. Schematic illustration of antigen-loaded UCNPs for DC stimulation, tracking, and vaccination in DC-based immunotherapy.

cell carcinoma,[8] and B cell lymphoma.[9] In this regard, efficient delivery of antigens into DCs, stimulation of DCs to induce their maturation, and the subsequent strong cross-presentation of tumor-specific antigens on DC membranes are essential requirements for DC-based immunotherapy.

On the other hand, in order to initiate specific immune responses by DC vaccines, antigen-stimulated DCs must migrate to draining lymph nodes, where they can interact with T cells.[10] The progress of migration, which is an essential process for DC-based vaccines to exert their functions, is usually studied by a traditional method known as "FITC painting".[11,12] Unfortunately, real-time imaging of DC migration cannot be realized with this technique, as it requires cutting out of tissues and staining. Various noninvasive imaging methods have thus been developed for DC tracking in both fundamental research and clinic trials, including the use of magnetic resonance imaging (MRI),[13,14] scintigraphy,[15] positron emission tomography (PET),[16] and fluorescence imaging.[17] Despite significant progress in this field, highly sensitive and accurate monitoring of DC migration *in vivo* remains challenging owing to the limitations of current imaging techniques and probes.

In recent years, near-infrared (NIR) excited upconversion nanoparticles (UCNPs) have attracted great attention due to their remarkable potential in biomedicine.[18−23] Distinguished from conventional downconversion photoluminescent probes, UCNPs could convert two or more low-energy photons to a single high-energy output photon under NIR excitation in the progress of upconversion luminescence (UCL). Therefore, UCNPs have many advantages in imaging such as minimal autofluorescence background signals and high resistance to photobleaching, which make them suitable for sensitive detection and imaging in complicated biological samples.[24−26] In our previous studies, ultrasensitive *in vivo* stem cell tracking with a detection limit down to as few as 10 cells in a mouse has been realized by labeling cells with UCNPs.[27,28] Therefore, we hypothesize that engineered UCNPs loaded with antigens may be used to label and stimulate DCs, which after being administrated into animals could be tracked by *in vivo* UCL imaging and finally realize DC-based immunotherapy with high efficiency.

In this work, we developed an advanced DC vaccine utilizing antigen-coated UCNPs to treat DCs (Scheme 1). UCNPs exhibiting strong UCL signals were synthesized and functionalized with polyethylene glycol (PEG) and polyethylenimine (PEI) to form dual-polymer-coated UCNP-PEG-PEI (UPP) nanoparticles. As the model antigen, chicken egg ovalbumin (OVA) was chosen and loaded onto UPP nanoparticles by electrostatic interaction. It was found that DCs after being treated with the UPP@OVA complex were stimulated to a higher maturation level with enhanced secretion of cytokines related to cellular immunity. Ultrasensitive *in vivo* detection of DCs (as few as ~50 DCs in a mouse) was then realized by UCL imaging, which also revealed the homing process of labeled DCs from peripheral tissue to draining lymph nodes. Importantly, compared to an OVA-pulsed DC vaccine, a UPP@OVA-pulsed DC vaccine induced stronger antigen-specific immune responses such as enhanced T cell proliferation, interferon gamma (IFN-γ) production, and cytotoxic T lymphocyte (CTL)-mediated response. This work for the first time realized highly sensitive *in vivo* DC tracking and a fabricated antigen-pulsed DC vaccine with robust immunities using antigen-loaded UCNPs, which may have great potential in the development of trackable DC-based immunotherapy.

RESULTS AND DISCUSSION

The UPP@OVA complex was prepared beginning with the synthesis of the UCNP core followed by coating of polymers and OVA protein (Figure 1a). First, Yb and Er-doped NaY/GdF_4 UCNPs (Y:Gd:Yb:Er = 58%:20%:20%:2%) were synthesized following a previous method with slight modifications.[29,30] Transmission electronic microscopy (TEM) images revealed that as-made UCNPs were monodispersed nanocrystals

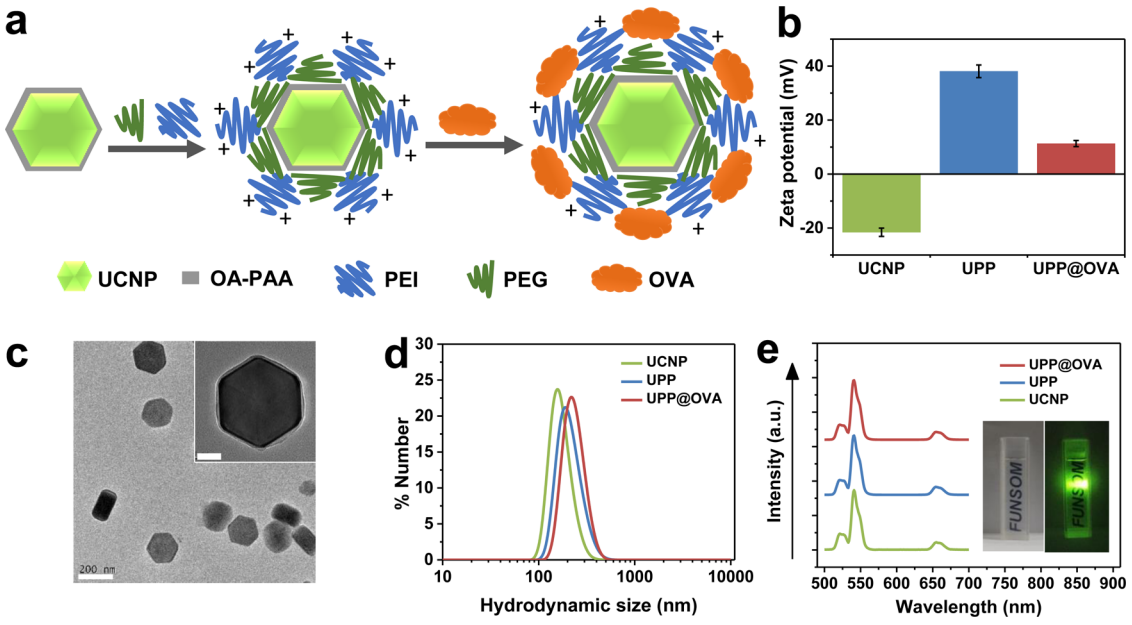

Figure 1. Characterization of antigen-loaded UCNPs (UPP@OVA). (a) Schematic illustration of the preparation process of UPP@OVA. (b) Zeta potentials of UCNP, UPP, and UPP@OVA. (c) TEM image of UPP@OVA (scale bar = 200 nm). Inset: A higher resolution TEM image of UPP@OVA (scale bar, 50 nm). (d) Hydrodynamic sizes of UCNP, UPP, and UPP@OVA. (e) UCL spectra of UCNP, UPP, and UPP@OVA at the same Y^{3+} concentration. Inset: Photographs of a UPP@OVA solution under an external 980 nm laser source (right) or ambient light (left).

with an average diameter of 170 nm (Supporting Figure S1a). The line profiles of elemental composition determined by energy-dispersive X-ray spectroscopy (EDS) further demonstrated the existence of Y, Gd, Yb, and Er elements within a single particle (Supporting Figure S1b). The X-ray diffraction (XRD) analysis of the as-prepared UCNPs nanocrystals showed that all peaks could be indexed to hexagonal structured UNCPs (JCPDS card, No.28-1192) (Supporting Figure S1c). To transfer those nanoparticles into the aqueous phase, UCNPs were then modified with octylamine-grafted poly(acrylic acid) (OA-PAA) polymer. The obtained nanoparticles with abundant carboxyl groups on their surface were then conjugated with both amine-terminated polyethylene glycol, which is a hydrophilic biocompatible polymer, and a cationic polymer polyethylenimine. The obtained dual-polymer-coated UCNP-PEG-PEI nanoparticles exhibited excellent solubility and stability in various physiological solutions, including saline, culture medium, and serum (Supporting Figure S2) and were highly positively charged (Figure 1b), as the result of both PEG and PEI coatings on their surface, respectively.

With an isoelectric point (pI) of 4.7, the model antigen OVA protein would exhibit negative charges under physiological pH and thus could be adsorbed onto the positively charged surface of UPP nanoparticles. Indeed, it was found that OVA could be effectively loaded on UPP nanoparticles by simply mixing UPP with OVA, and the saturated OVA loading on UPP nanoparticles was determined to be ~10% (w/w) by the bicinchoninic acid (BCA) protein assay (Supporting Figure S3).

We then carefully characterized the obtained UPP@OVA complex. TEM images clearly revealed a layer of polymer/protein shell on the UCNP core for the UPP@OVA complex (Figure 1c). As expected, the hydrodynamic sizes of nanoparticles showed a slight increase after the polymer modification and protein loading (Figure 1d). Meanwhile, UPP@OVA appeared to be highly stable in physiological solutions (Figure 1e). Under excitation by a 980 nm NIR laser, UPP@OVA showed strong UCL emission signals, which were not affected by polymer coating and protein loading (Figure 1e). Therefore, our results demonstrated that it could be feasible to utilize UPP@OVA for antigen delivery into DCs and the subsequent tracking.

Next, we studied how UPP@OVA would interact with DCs. Phagocytic immature DCs were obtained from C57BL/6 mice following the established protocol.[31] To study the potential cytotoxicity of nanoparticles, DCs were treated with various concentrations of UPP or UPP@OVA (Supporting Figure S4). It was found that those nanoparticles did not exert significant cytotoxicity to DCs within our tested concentration range (12.5−100 μg/mL).

In order to investigate the delivery progress of UPP@OVA into DCs, OVA was prelabeled by a fluorescent dye (FITC) and used to form the UPP@OVA complex, which was then incubated with DCs. Confocal fluorescent microscope images clearly revealed the nice colocalization of FITC-OVA fluorescence and UCL signals inside the cells (Figure 2a), suggesting that OVA was effectively delivered into the DCs by UPP. Confocal

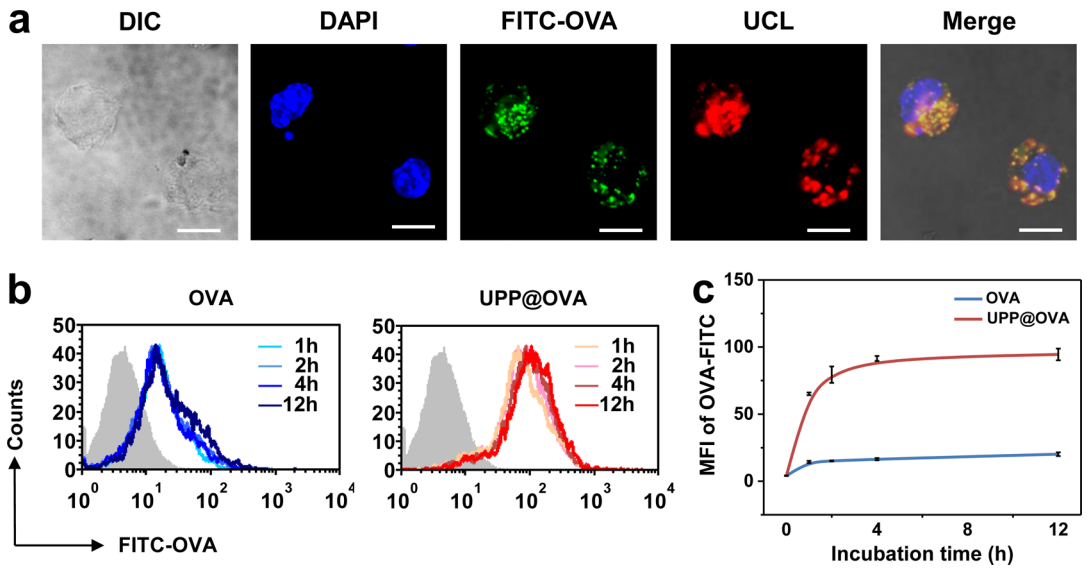

Figure 2. Intracellular delivery of UPP@OVA into DCs. (a) Confocal images of UPP@OVA-pulsed DCs. DIC, differential interference contrast. UCL signals (red) were from the UCNP core, while OVA (green) were prelabeled with FITC. Nuclei (blue) were stained with DAPI. Scale bar = 10 μm. (b) Flow cytometric analysis of FITC-labeled OVA in DCs incubated with OVA or UPP@OVA. (c) Mean fluorescence intensity (MFI) of FITC-OVA from DCs sample in (b).

fluorescence images of LysoTracker Red-stained cells further confirmed that those nanoparticles were internalized by DCs, likely *via* endocytosis (Supporting Figure S5). The quantitative flow cytometry measurement was then conducted to monitor the internalization of FITC-OVA in the nanoparticle formulation or its free form. It was uncovered that the DC uptake of OVA was dramatically enhanced by nearly 5-fold when OVA was loaded on UPP (Figure 2b,c, Supporting Figure S6), demonstrating that our nanoparticles could serve as a rather effective antigen-delivery platform for DCs. Considering the accelerated release of OVA from nanoparticles under lower pH (*e.g.*, lysosomal pH) (Supporting Figure S7), and the existence of proteases in cellular endosomes/lysosomes, OVA delivered into cells may be detached from UPP and then processed by DCs as an antigen.

Immature DCs act as antigen-capturing cells, whereas mature DCs mainly function as antigen-presenting cells.[5] After capturing the antigen/pathogen, DCs will process the antigen into peptides during the migration, present peptide-major histocompatibility complex (MHC) complex to naive T cells upon arriving at draining lymph nodes, and finally initiate subsequent immune responses.[32] The level of DC maturation, which could be indicated by the upregulation of co-stimulatory molecules (CD80, CD86) on their membrane, is thus a quite important index to evaluate the immune response in DC-based immunotherapy.[33] In our experiments, it was found that the percentage of matured DCs ($CD11c^+CD80^+CD86^+$) remarkably increased from 27.72 $\pm$ 0.34% to 50.47 $\pm$ 3.22% after treatment with UPP@OVA, while the DC maturation level of those treated by the same dose of free OVA was only increased to 41.9 $\pm$ 3.08% (Figure 3a,b), suggesting that UPP@OVA-stimulated DCs may induce much stronger immune responses.

The soluble cytokines secreted by DCs would vary at different stages of DC development and maturation and could regulate other immune cells and mediate subsequent immune responses.[34] It has been demonstrated that an interleukin 12 (IL-12p70)-producing DC vaccine is able to elicit strong therapeutic T helper type 1 (Th1) antigen-specific $CD8^+$ T cell immunity in patients,[35,36] while interleukin 1β (IL-1β) plays an important role in the activation of natural killer cells for efficient priming of Th1 cells and CTLs.[37] The secretion of IL-12p70 and IL-1β in supernatants of DCs after various treatments was analyzed by an enzyme-linked immunosorbent assay (ELISA) in our experiments (Figure 3c,d). Compared to samples treated with free UPP or OVA, the levels of IL-12p70 and IL-1β secreted by DCs showed a significant increase after UPP@OVA treatment. Our results taken together suggest that the model antigen, OVA protein, could be effectively delivered into DCs with the help of UPP nanoparticles, resulting in DC maturation and enhanced cytokine release. These activated DCs, or so-called antigen-pulsed DC vaccines, could then be used for DC-based immunotherapy.

In our previous work, we have demonstrated UCNPs could be employed for *in vivo* stem cell tracking with an ultrahigh sensitivity.[28] In order to realize *in vivo* DC tracking, we first studied the *in vivo* detection sensitivity of UPP@OVA-labeled DCs. Various amounts of labeled DCs were injected into the back of C57BL/6 mice with hair removed, which were then imaged with a modified *in vivo* imaging system using an external 980 nm laser as the excitation source. Note that under our imaging conditions the heating of mouse skin

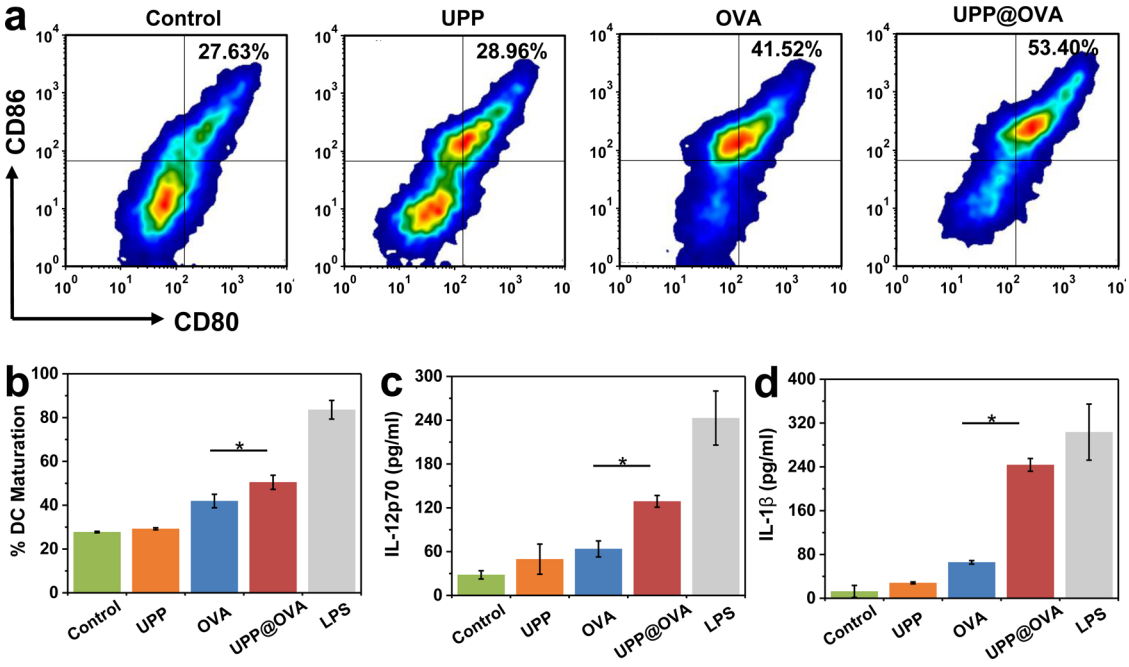

Figure 3. Enhanced DC matration and cytokine release after UPP@OVA treatment. (a, b) Quantification of $CD80^+$ and $CD86^+$ expression, which are markers for DC maturation on the surface of DCs ($CD11c^+$) after *in vitro* incubation with OVA, UPP, or UPP@OVA for 12 h by flow cytometry. Lipopolysaccharide (LPS) treatment was the positive control. (c, d) Secretion of IL-12p70 (c) and IL-1β (d) in suspensions of samples in (b) measured by an ELISA assay. Data are presented as the mean $\pm$ standard errors of the mean (SEM) (*$p < 0.05$).

exposed to the 980 nm laser was insignificant and induced no harm to the imaged animal (Supporting Figure S8). Strong UCL signals were observed from the injection sites (Figure 4a). The quantitative analysis of imaging data showed that the UCL signals were stronger with increasing amounts of implanted DCs (Figure 4b). Impressively, as few as ~50 DCs injected into a mouse could be clearly seen under UCL imaging. It is worth noting that cell labeling by other types of nanoprobes, such as fluorescent quantum dots (QDs) or magnetic nanoparticles, usually can only enable *in vivo* tracking of no less than thousands of cells in mice.[38,39] Highly sensitive *in vivo* DC tracking would provide valuable information to understand how stimulated DCs would migrate and work in DC-based immunotherapy.

In DC-based immunotherapy, it is necessary for antigen-loaded DCs to migrate from injection sites to draining lymph nodes through lymphatic vessels.[10] Hence, UPP@OVA-labeled DCs were injected into the right footpad of C57BL/6 mice to simulate the progress of DC migration. The signals from labeled DCs were monitored by the *in vivo* imaging system after administration. UCL signals appeared in the popliteal lymph node 36 h post injection (pi) of UPP@OVA-labeled DCs and became quite strong at 48 h pi, indicating gradual migration of UPP@OVA-labeled DCs from the injection site to the draining lymph node through lymphatic vessels (Figure 4c, Supporting Figure S9). *Ex vivo* imaging of popliteal lymph nodes dissected from both sides of the mouse confirmed that the observed UCLs signals were indeed from the draining lymph node on the side where DCs were injected (Figure 4d).

It is known that activated DCs will mainly migrate to the T cell zone in draining lymph nodes to interact with native T cells.[40] We thus collected the popliteal lymph node for immunofluorescence staining with Thy1.2 and B220 to distinguish the T cell zone and the B cell zone, respectively. The confocal images of lymph node slices showed that most of the UCL signals were exclusively from the T cell zone, but not found in the B cell zone (Figure 4e). As the control, UCL signals appeared in both zones of the lymph node when free UPP@OVA nanoparticles were injected into mice, further confirming that the observed UCL signals in the lymph nodes of DC-injected mice were from UPP@OVA-labeled DCs that migrated into the lymph node instead of free nanoparticles leaked out of DCs (Figure S6). The ability of DCs to migrate into draining lymph nodes is the basic requirement for DCs to exert their functions. Our results thus indicated that UPP@OVA-labeled DCs remained active after being administrated back into animals.

In order to explore whether a UPP@OVA-pulsed DC vaccine is able to trigger a corresponding immune response *in vivo*, C57/BL6 mice were vaccinated with UPP@OVA-pulsed DCs, OVA-pulsed DCs, or fresh DCs two times at a week interval (Figure 5a). After intradermal injection (id) at the base of the tails, strong UCL signals were mainly found in swollen inguinal lymph nodes as revealed by *ex vivo* UCL imaging, suggesting that labeled DCs would migrate to nearby

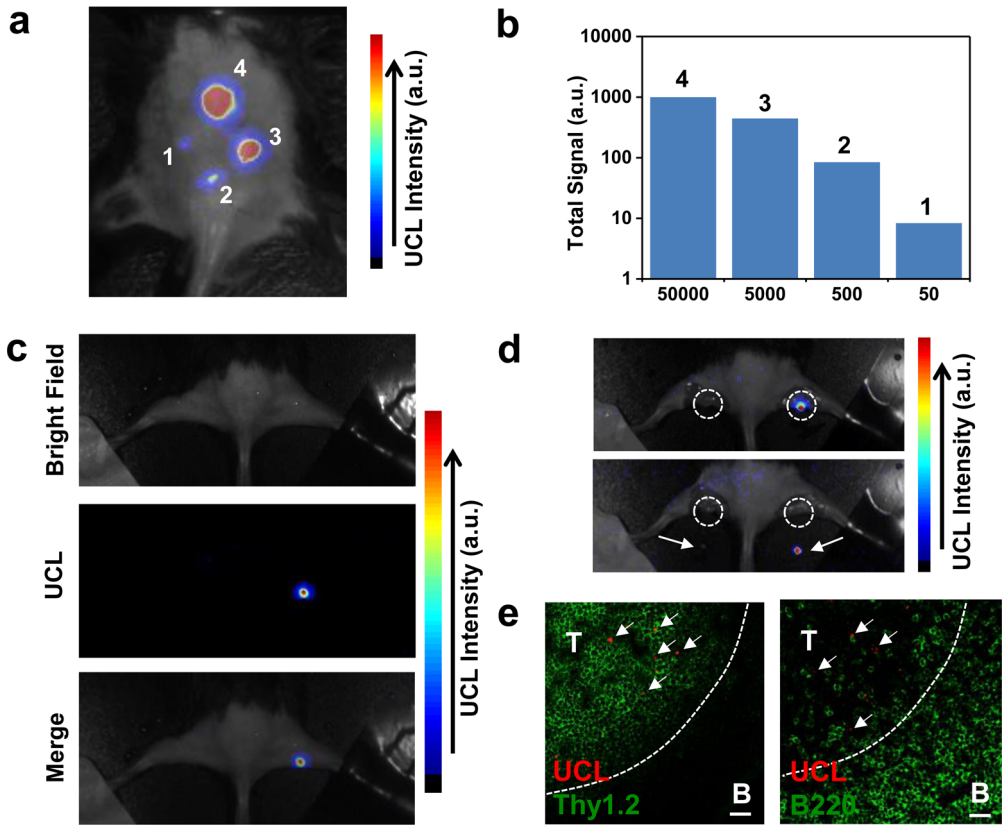

Figure 4. *In vivo* **tracking of UCNP@OVA-labeled DCs. (a) UCL image of a C56BL/6 mouse subcutaneously injected with various numbers of labeled DCs (≈ 50 to 50 000). (b) Quantification of UCL signals in (a). (c−e) DC migration from footpad to draining lymph node. (c) Labeled DCs were injected into the right footpad of a mouse; 48 h after injection, strong UCL signals from the draining lymph node were seen under** *in vivo* **UCL imaging. (d)** *Ex vivo* **imaging of popliteal lymph nodes (white circles) before (top) and after (bottom) being dissected from the mouse. (e) Immunofluorescence images of the lymph nodes dissected from the mouse injected with UPP@OVA-labeled DCs. T: T-cell zone (Thy1.2$^+$). B: B-cell zone (B220$^+$). Scale bar = 20 μm. Arrows point to UCL signals from labeled DCs.**

lymph nodes to initiate immune responses (Supporting Figure S10).

Different from innate immunity, adaptive immunity is featured by the rapid occurrence of stronger T cell-mediated immune responses within a short time upon the second exposure to the same pathogen.[41] During this process, T cells will greatly expand to eliminate pathogen/pathogen-infected cells (*e.g.*, cancer cells). Therefore, the proliferation capability of T cells is one of the most important parameters to evaluate the vaccine-induced immune response.[42,43] The model antigen that we chose is a well-characterized target antigen to induce CD8 T cell immunity (OVA peptide 257−264).[44] On the basis of flow cytometry data of carboxyfluorescein succinimidyl ester (CFSE)-stained T cells, it was found that T cells from mice immunized with UPP@OVA-pulsed DCs exhibited greater proliferation capability compared with other control groups (Figure 5b,c). Meanwhile, we also tested the immune response triggered by free antigen or UPP@OVA alone without DCs *via* the T cell proliferation index. It was uncovered that neither antigen alone nor UPP@OVA by itself could significantly enhance the T cell proliferation capability, further demonstrating the advantages of DC vaccines in triggering stronger immune responses (Supporting Figure S11).

Cellular immunity is greatly necessary for the treatment of cancers and endogenous pathogen infectious diseases. It is well known that interferon gamma (IFN-γ) and tumor necrosis factor alpha (TNF-α), which are typical markers of cellular immunity, play critical roles in the immunotherapy against cancer.[45−47] In this study, the secretion of IFN-γ from T cells as determined by the enzyme-linked immunospot assay (ELISPOT) was remarkably enhanced after treatment by UPP@OVA-pulsed DCs, in marked comparison to that of the OVA-pulsed DCs immunization group (Figure 5d). Meanwhile, the production level of TNF-α in serum also showed a significant increase when mice were immunized with UPP@OVA-pulsed DCs (Figure 5e), suggesting cellular immunity was successfully induced by our DC vaccine.

CTLs are a type of T lymphocytes derived from CD8$^+$ T cells that can be activated after binding to an antigen-specific class I MHC molecule.[48,49] Their main function is to kill cancer cells or infected cells *via* releasing cytotoxins such as perforin and granzymes.[50,51] In this study, splenocytes (containing CD4$^+$ T cells,

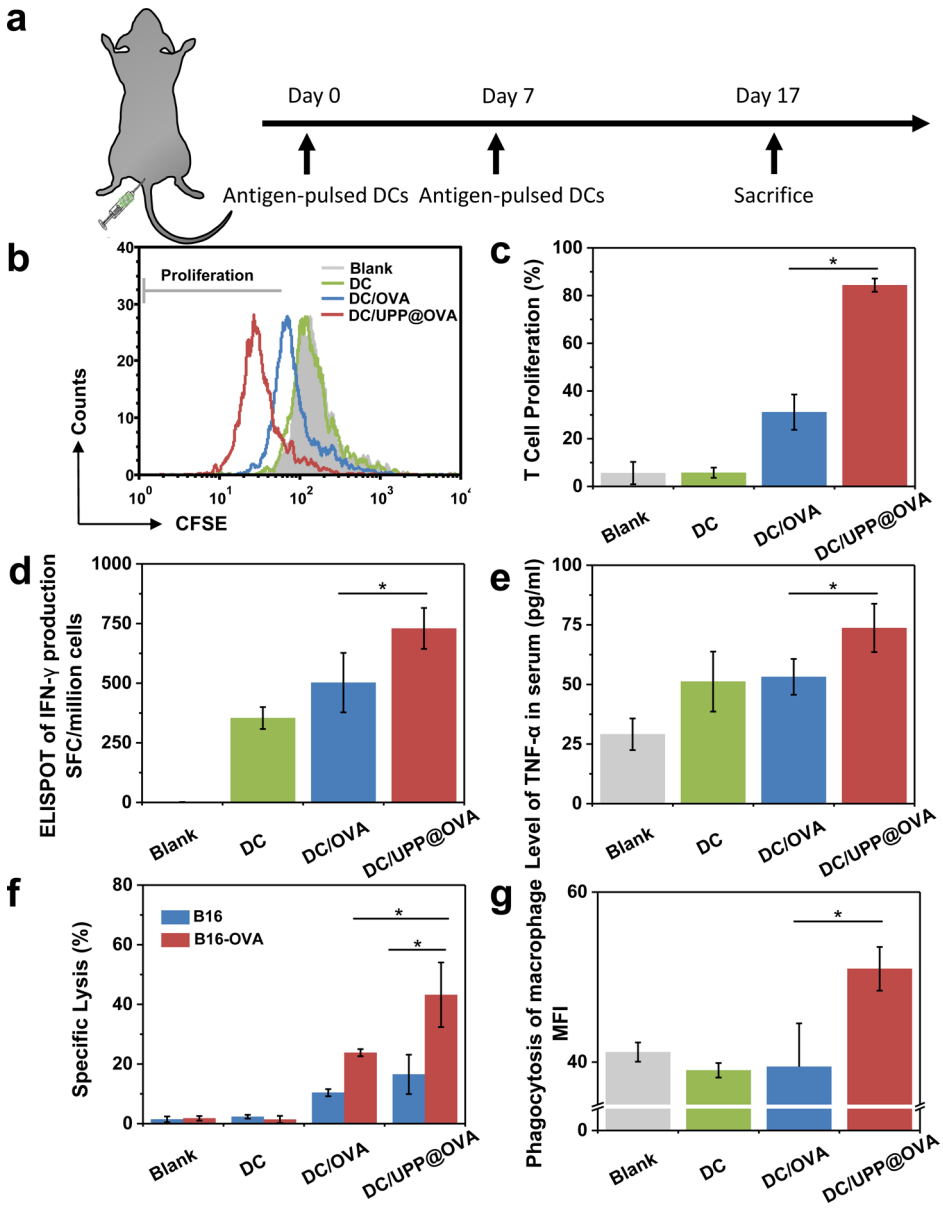

Figure 5. *In vivo* **immune responses after administration of DC vaccines. (a) Scheme showing the experimental design. C57BL/6 mice divided into several groups were vaccinated twice with PBS, DCs, OVA-pulsed DCs, or UPP@OVA-pulsed DCs at a week interval and then sacrificed 10 days later to harvest spleen, serum, and macrophages for analysis. (b, c) T cell proliferation capability of immunized mice detected by flow cytometry. (d) IFN-γ production secreted from restimulated splenocytes detected by an ELISPOT assay. (e) Level of TNF-α in serum. (f) CTL-mediated immune responses measured by incubating restimulated splenocytes with B16 or B16-OVA tumor cells. (g) Phagocytosis capability of primary macrophage. Data are presented as the mean $\pm$ SEM (*$p < 0.05$).**

$CD8^+$ T cells, B cells, *etc.*) harvested from immunized mice were treated with OVA protein for 3 days to activate the memory T cells and then incubated with B16 melanoma cells or its OVA-expressing derivative (B16-OVA) to evaluate the cytotoxicity mainly mediated by CTLs to tumor cells (Figure 5f).[52] The results were inspiring, as obviously enhanced cytotoxic responses induced by CTLs in splenocytes against B16-OVA cancer cells were observed in the UPP@OVA-pulsed DC vaccine group when compared to other control groups. In contrast, the cytotoxicity of CTLs against normal B16 cancer cells was not significant in any tested group. All the *in vivo*/*ex vivo* data from different perspectives demonstrated that a UPP@OVA-pulsed DC vaccine was able to induce robust antigen-specific immune responses to selectively destruct cancer cells with that antigen overexpression, promising for cancer immunotherapy.

In addition to adaptive immunity, innate immunity also plays important roles in combating tumor growth at the early stage and could regulate the activity of adaptive immunity. In consideration of the crucial roles of macrophages in innate immunity, in this study, the phagocytosis capability of primary peritoneal

macrophages was evaluated using latex beads. It was found that macrophages from mice immunized with UPP@OVA-pulsed DCs could engulf more beads than those from the OVA-pulsed DCs group (Figure 5g). As DCs are described as versatile controllers of the immune system and act as messengers between the innate and adaptive immune system,[2] the UPP@OVA-pulsed DC vaccine may not only promote adaptive immune responses but also stimulate innate immune responses, thus giving the whole body a better situation to prevent pathogen or virus invasions.

CONCLUSION

In summary, we have developed antigen-loaded UCNPs for DC stimulation, tracking, and vaccination for DC-based immunotherapy in this work. On one hand, the dual-polymer-coated UCNPs could be utilized as effective nanocarriers that dramatically enhance the uptake of OVA in DCs and further induce DC maturation and cytokine release. On the other hand, the fantastic optical properties of UCNPs could be taken advantage of to monitor the *in vivo* translocation of DCs with high sensitivity. Furthermore, DCs pulsed with the nanoparticle–antigen complex (UPP@OVA) could serve as an effective DC vaccine and trigger a strong antigen-specific immune response including enhanced T cell proliferation, IFN-γ secretion, and CTL-mediated responses in immunized mice, showing remarkably improved efficiency compared to DCs pulsed by free OVA or a nanoparticle–antigen complex in the absence of DCs. Our work is the first example of applying UCNPs in trackable DC-based immunotherapy, which features great *in vivo* tracking sensitivity and highly effective antigen-specific immune responses, which are promising for future immunotherapy treatment against major diseases including cancer.

MATERIALS AND METHODS

1. Synthesis of UCNP-PEG-PEI. NaY/GdF_4:Yb:Er upconversion nanoparticles (Y:Gd:Yb:Er = 58%:20%:20%:2%) were synthesized by a typical thermal decomposition method following our previously reported procedure.[21] UCNP-PEG-PEI nanoparticles was fabricated also according to our previous work.[30] Briefly, the hydrophobic as-made UCNPs were first modified with an OA-PAA polymer, which was synthesized following a literature protocol,[53] resulting in UCNP-PAA dispersed in water. The UCNP-PAA was further conjugated with PEG by mixing 1 mg/mL of UCNP-PAA with 2 mg/mL of six-armed amine-terminated PEG (10 kDa, Sun-Bio Inc.) under sonication for 5 min and then adding 1 mg/mL of 1-ethyl-3-(3-dimethylaminoropyl) carbodiimide hydrochloride (EDC) (Sigma-Aldrich) to induce amide formation. After being stirred for 20 min, 5 mg/mL of PEI (10 kDa, Sigma-Aldrich) and another batch of EDC (2 mg/mL) were added to the solution, which was stirred at room temperature overnight and then purified by centrifugation. The obtained UPP was resuspended in water for future use.

2. Characterization of Nanoparticles. Transmission electron microscopy and high-resolution TEM images were obtained using a FEI Tecnai F20 transmission electron microscope. The phase and crystallography of the products were characterized by using a PANalytical X-ray diffractometer. UCL spectra were obtained on a FluoroMax 4 luminescence spectrometer (HORIBA Jobin Yvon) under excitation with an external 980 nm laser (1 W, continuous wave, Beijing Hi-Tech Optoelectronics Co., Ltd.). The concentrations of UCNPs were measured by inductively coupled plasma mass spectrometry (ICP-AES). Zeta potentials and hydrodynamic sizes of various nanoparticles were measured by a Nano-ZS90 nanoparticle analyzer (Malvern Instruments Co., Ltd.).

3. Loading Capacity and Release of OVA. UPP@OVA was obtained after loading ovalbumin protein (Sigma) on the surface of UPP *via* electrostatic interaction. To test the loading capacity of OVA on nanoparticles, various concentrations of OVA were added into the UPP solution (1 mg/mL) and incubated for 20 min. Then the mixtures were centrifuged at 14 800 rpm for 5 min to remove unattached OVA. The quantity of OVA loaded on UPP was measured by the bicinchoninic acid protein assay (Thermo) according to the vendor's instructions. To investigate the release of OVA from UPP in a biological system, UPP@OVA nanoparticles were dispersed in sodium citrate buffer solution (20 mM, pH = 5.0) or phosphate buffer solution (20 mM, pH = 7.4) and then incubated for various periods of time. The released OVA was measured by the BCA protein assay after separation *via* centrifugation.

4. Animals and Cells. Eight-week-old female C57BL/6 mice purchased from Nanjing Peng Sheng Biological Technology Co., Ltd. were used under protocols approved by Soochow University Laboratory Animal Center. The B16 melanoma cell line and its derivative expressing OVA (B16-OVA), which were kindly provided by Prof. Haiyan Liu (Soochow University, China), were cultured and maintained in Dulbecco's modified Eagle medium (HyClone) supplemented with 10% heat-inactivated fetal bovine serum (FBS) and 1% penicillin–streptomycin under 37 °C in 5% CO_2.

Dendritic cells were generated from the bone marrow (BM) of 8- to 10-week-old C57BL/6 mice according to an established method.[31] Briefly, the bone marrow was obtained by flushing the femur and tibia with Roswell Park Memorial Institute (RPMI) 1640 medium (HyClone) containing 10% FBS. After treating with red blood cell lysis solution (Cwbiotech), 1×10^6 BM cells were seeded in each 60 mm bacteriological Petri dish with 3 mL of culture medium containing 20 ng/mL granulocyte-macrophage colony-stimulating factor (GM-CSF, PeproTech) and 50 μM β-mercaptoethanol (Sigma). On day 3, an additional 4 mL of the same medium was added into these plates. On day 6, half of the culture supernatant was collected and centrifuged. Cells were added back into the original plates with media containing GM-CSF. On day 8, BM-DCs were obtained for further use.

5. Cell Viability Assay. Cell viability was measured by the 3-(4,5-dimethyl-2-thiazolyl)-2,5-diphenyl-2*H*-tetrazolium bromide (MTT) assay (Sigma). DCs (1×10^5 cells) were incubated with various concentrations of UPP or UPP@OVA for 24 h. After removing nanoparticles in suspension, MTT (0.5 mg/mL) diluted in fresh cell medium was added to each well for another 4 h at 37 °C. After adding dimethyl sulfoxide to solubilize the formazan, the absorbance of each sample at 560 nm was measured using a microplate reader (Bio-Rad).

6. Confocal Imaging. To study the localization of UPP@OVA in DCs, OVA was prelabeled with fluorescein isothiocyanate (FITC) before the UPP@OVA complex was prepared. On day 8 of the culture, DCs were incubated with UPP@OVA for 4 h, fixed with paraformaldehyde, and then stained with 4′,6-diamidino-2-phenylindole (DAPI). Confocal luminescence imaging of DCs was obtained with a modified Olympus laser-scanning microscope using a 980 nm external laser as the excitation source. The UCL signals of UPP from 500 to 700 nm were recorded by the microscope. All the color from various dyes was the artificial color processed by the software in confocal images. For

lysosome staining, DCs were incubated with LysoTracker Red DND-99 (Life Technology, Cat. L7528) for 30 min before harvesting the treated DCs for confocal imaging.

7. Flow Cytometry (FACS) Assay. To detect intracellular OVA signals, FITC-OVA alone or UPP@OVA containing FITC-OVA was incubated with DCs for different periods of time (0, 1, 2, 4, 12 h) at a final OVA concentration of 2.5 μg/mL. After washing the DCs with FACS buffer (phosphate buffer saline (PBS) containing 1% FBS), the cellular fluorescence was measured by FACS analysis (BD FACSCalibur).

To measure the maturation level of DCs after various treatments, DCs were washed with FACS buffer and subsequently stained with anti-CD11c-FITC, anti-CD86-PE, and anti-CD80-APC antibodies (eBioscience) for 20 min at room temperature. These DCs were then sorted by flow cytometry after being washed again with FACS buffer. All samples were done in triplicate.

8. Cytokine Detection. The suspension of DC culture media and serum samples isolated from mice after various treatments were diluted for analysis. interleukin-1β (IL-1β), interleukin 12 (IL-12p70), and tumor necrosis factor α (TNF-α, Dakewe Biotech) were analyzed with cytokine-specific ELISA kits respectively according to the vendor's instructions. All samples were measured in triplicate.

9. *In Vivo* UCL Imaging. To test the *in vivo* tracking sensitivity, UPP@OVA-labeled DCs (5×10, 5×10^2, 5×10^3, and 5×10^4 cells) diluted in PBS were subcutaneously transplanted into the back of C57BL/6 mice with hair removed. A modified Maestro *in vivo* imaging system using a 980 nm laser as the excitation source was utilized to obtain UCL signals from mice. The laser power density was $\sim$1 W/cm^2 during imaging (exposure time = 30 s). Meanwhile, in order to prevent the interference of excitation light with the CCD camera, an 850 nm short-pass emission filter was applied. For *in vivo* DC tracking, UPP@OVA-labeled DCs (1×10^6) were subcutaneously injected into the hind-leg footpad of a C57BL/6 mouse. UCL imaging of the injected mouse was performed at 0, 12, 24, 36, and 48 h after DC administration. Further, popliteal lymph nodes were cut out to confirm the source of the signals under the same imaging system. The thermal effect of UCL imaging was monitored by an IR thermal camera (IRS E50 ProThermal imaging camera) during the whole imaging process.

10. Immunofluorescence. After *in vivo* UCL imaging, the popliteal lymph nodes were dissected at 48 h post DC administration. They were then fixed with 4% paraformaldehyde, embedded in O.C.T. compound (Tissue-Tek), frozen in liquid nitrogen, and finally stored at -80 °C until staining. Cryosections (10 μm thick) were prepared on gelatin-coated microscope slides and baked in an oven for 1 h at 55 °C. Lymph node sections were blocked with 5% bovine serum albumin (BSA) followed by incubation with primary antibodies against Thy1.2 and B220 (Biolegend) at 4 °C overnight. After extensive washing with PBST (PBS containing 0.05% Tween-20), sections were incubated with fluorescent secondary antibodies (Jackson ImmunoResearch, cat. 112-095-143) for 1 h at 37 °C in the dark and then mounted for confocal imaging.

11. T Cell Proliferation Assay. In order to get different types of DC vaccines, DCs were incubated with OVA, UPP, or UPP@OVA for 12 h at the final OVA concentration of 10 μg/mL. Mice were divided into several groups (n = 6) and immunized with PBS, untreated DCs, OVA-treated DCs, UPP-treated DCs, or UPP@OVA-treated DCs (2×10^6) through intradermal injection. Mice from different groups were immunized twice at a week interval. Ten days after the last immunization, spleen, serum, and primary macrophages were obtained for further analysis. Splenocytes (1×10^6 cells) harvested from various groups were stained with the CellTrace CFSE cell proliferation kit (Invitrogen) according to the vendor's protocol. Cells were carefully washed three times with cell culture medium and incubated in the presence OVA peptide (257$-$264, Invivogen) at a concentration of 3 μg/mL for 3 days. The background proliferative responses were determined by culturing cells in the absence of OVA peptides. Cells were then stained with anti-CD3e antibody (eBioscience) for 30 min at room temperature. After being washed with FACS buffer, the CFSE-stained cells were sorted by flow cytometry. All samples were done in triplicate. Mice were also immunized with 200 μL of PBS, OVA, UPP, or UPP@OVA at the OVA concentration of 5 μg/mL, which should be much higher than the total OVA content in UPP@OVA-labeled DCs injected into mice, to evaluate T cell proliferation with the same method described before.

12. ELISPOT Assay. An ELISPOT set (BD-Biosciences, cat. 551083) was utilized to detect IFN-γ secreted by splenocytes according to the vendor's protocol. Initially, the ELISPOT plates were coated with anti-IFN-γ antibody at 5 μg/mL, incubating overnight at 4 °C, and then blocked with cell culture medium for another 2 h at room temperature. Total splenocytes (5×10^5) from immunized mice were added in each well and cultured in the presence of 5 μg/mL OVA peptide. Phorbol 12-myristate 13-acetate and ionomycin were used as the positive control. After incubation for 24 h, the plates were washed and incubated with biotinylated anti-IFN-γ antibody for 2 h at room temperature, followed by adding HRP-conjugated avidin and incubating for another 1 h. Chromogenic reactions occurred when adding 3-amino-9-ethylcarbazole substrate (BD-Biosciences, cat. 551951) into the plates after removing unattached avidin. Quantification of IFN-γ spot-forming cells (SFC) was measured using an Immunospot Analyzer ELISPOT reader (Cellular Technologies Ltd.). Data are presented as SFC/10^6 cells.

13. Cytotoxic T Lymphocyte Activity. Splenocytes harvested from mice were restimulated with 40 μg/mL purified OVA protein for 3 days in RPMI 1640. The cells were washed three times with PBS to completely remove residual protein and then cultured together with B16 or B16-OVA target cells (5×10^3 cells/well) in 96-well culture plates at the effective target cell ratio of 100:1. After 4 h of incubation, the suspensions were collected to detect the LDH leakage level with a nonradioactive cytotoxicity assay (Promega, cat. 7891), which indicated the level of specific lysis of target cells by effective cells. The percentage of specific lysis was calculated according to % specific lysis = ((experimental LDH release $-$ effective cell LDH release)/(maximum LDH release $-$ spontaneous LDH release)) $\times$ 100%.

14. Phagocytosis Capability of Primary Macrophages. In order to explore the effects of DC vaccines on phagocytosis capability of primary macrophages, fluorescence microbeads (Sigma, cat. L9904) were utilized to incubate with macrophages harvested from immunized mice for 12 h at a concentration of 0.6 μg/mL. The macrophages were then sorted by flow cytometry after being washed with FACS buffer.

15. Statistical Analysis. For statistic comparison, a p value, which was calculated by the Student's t test, of less than 0.05 was considered to be statistically significant.

Conflict of Interest: The authors declare no competing financial interest.

Supporting Information Available: Supporting Figures S1$-$11. The Supporting Information is available free of charge on the ACS Publications website at DOI: 10.1021/acsnano.5b02014.

Acknowledgment. This work is supported by the National Basic Research Program of China (973 Program, 2012CB932601 and 2011CB911000), National Natural Science Foundation of China (31300824, 51302180, 51222203), the National Natural Science Foundation of Jiangsu Province (BK20130005), China Postdoctoral Science Foundation (2013M530267), and a Project Funded by the Priority Academic Program Development of Jiangsu Higher Education Institutions (PAPD).

REFERENCES AND NOTES

1. Liu, Y.-J. Dendritic Cell Subsets and Lineages, and Their Functions in Innate and Adaptive Immunity. *Cell* **2001**, *106*, 259–262.
2. Steinman, R. M. Dendritic Cells: Versatile Controllers of the Immune System. *Nat. Med.* **2007**, *13*, 1155–1159.
3. Kapsenberg, M. L. Dendritic-Cell Control of Pathogen-Driven T-Cell Polarization. *Nat. Rev. Immunol.* **2003**, *3*, 984–993.
4. Lu, W.; Arraes, L. C.; Ferreira, W. T.; Andrieu, J.-M. Therapeutic Dendritic-Cell Vaccine for Chronic HIV-1 Infection. *Nat. Med.* **2004**, *10*, 1359–1365.

5. Banchereau, J.; Palucka, A. K. Dendritic Cells as Therapeutic Vaccines against Cancer. *Nat. Rev. Immunol.* **2005**, *5*, 296–306.
6. Melief, C. J. Cancer Immunotherapy by Dendritic Cells. *Immunity* **2008**, *29*, 372–383.
7. Nestle, F. O.; Alijagic, S.; Gilliet, M.; Sun, Y.; Grabbe, S.; Dummer, R.; Burg, G.; Schadendorf, D. Vaccination of Melanoma Patients with Peptide- or Tumorlysate-Pulsed Dendritic Cells. *Nat. Med.* **1998**, *4*, 328–332.
8. Kugler, A.; Stuhler, G.; Walden, P.; Zöller, G.; Zobywalski, A.; Brossart, P.; Trefzer, U.; Ullrich, S.; Müller, C. A.; Becker, V.; *et al*. Regression of Human Metastatic Renal Cell Carcinoma after Vaccination with Tumor Cell-Dendritic Cell Hybrids. *Nat. Med.* **2000**, *6*, 332–336.
9. Hsu, F. J.; Benike, C.; Fagnoni, F.; Liles, T. M.; Czerwinski, D.; Taidi, B.; Engleman, E. G.; Levy, R. Vaccination of Patients with B-Cell Lymphoma Using Autologous Antigen-Pulsed Dendritic Cells. *Nat. Med.* **1996**, *2*, 52–58.
10. Randolph, G. J.; Angeli, V.; Swartz, M. A. Dendritic-Cell Trafficking to Lymph Nodes through Lymphatic Vessels. *Nat. Rev. Immunol.* **2005**, *5*, 617–628.
11. Ohl, L.; Mohaupt, M.; Czeloth, N.; Hintzen, G.; Kiafard, Z.; Zwirner, J.; Blankenstein, T.; Henning, G.; Förster, R. CCR7 Governs Skin Dendritic Cell Migration under Inflammatory and Steady-State Conditions. *Immunity* **2004**, *21*, 279–288.
12. Acton, S. E.; Astarita, J. L.; Malhotra, D.; Lukacs-Kornek, V.; Franz, B.; Hess, P. R.; Jakus, Z.; Kuligowski, M.; Fletcher, A. L.; Elpek, K. G.; *et al*. Podoplanin-Rich Stromal Networks Induce Dendritic Cell Motility *via* Activation of the C-Type Lectin Receptor CLEC-2. *Immunity* **2012**, *37*, 276–289.
13. De Vries, I. J. M.; Lesterhuis, W. J.; Barentsz, J. O.; Verdijk, P.; van Krieken, J. H.; Boerman, O. C.; Oyen, W. J.; Bonenkamp, J. J.; Boezeman, J. B.; Adema, G. J.; *et al*. Magnetic Resonance Tracking of Dendritic Cells in Melanoma Patients for Monitoring of Cellular Therapy. *Nat. Biotechnol.* **2005**, *23*, 1407–1413.
14. Cho, N.-H.; Cheong, T.-C.; Min, J. H.; Wu, J. H.; Lee, S. J.; Kim, D.; Yang, J.-S.; Kim, S.; Kim, Y. K.; Seong, S.-Y. A Multifunctional Core-Shell Nanoparticle for Dendritic Cell-Based Cancer Immunotherapy. *Nat. Nanotechnol.* **2011**, *6*, 675–682.
15. De Vries, I. J. M.; Krooshoop, D. J.; Scharenborg, N. M.; Lesterhuis, W. J.; Diepstra, J. H. S.; van Muijen, G. N.; Strijk, S. P.; Ruers, T. J.; Boerman, O. C.; Oyen, W. J.; *et al*. Effective Migration of Antigen-Pulsed Dendritic Cells to Lymph Nodes in Melanoma Patients Is Determined by Their Maturation State. *Cancer Res.* **2003**, *63*, 12–17.
16. Prince, H. M.; Wall, D. M.; Ritchie, D.; Honemann, D.; Harrrison, S.; Quach, H.; Thompson, M.; Hicks, R.; Lau, E.; Davison, J.; *et al*. *In Vivo* Tracking of Dendritic Cells in Patients with Multiple Myeloma. *J. Immunother.* **2008**, *31*, 166–179.
17. Noh, Y.-W.; Jang, Y.-S.; Ahn, K.-J.; Lim, Y. T.; Chung, B. H. Simultaneous *in Vivo* Tracking of Dendritic Cells and Priming of An Antigen-Specific Immune Response. *Biomaterials* **2011**, *32*, 6254–6263.
18. Wang, F.; Liu, X. Recent Advances in the Chemistry of Lanthanide-Doped Upconversion Nanocrystals. *Chem. Soc. Rev.* **2009**, *38*, 976–989.
19. Gai, S.; Li, C.; Yang, P.; Lin, J. Recent Progress in Rare Earth Micro/Nanocrystals: Soft Chemical Synthesis, Luminescent Properties, and Biomedical Applications. *Chem. Rev.* **2013**, *114*, 2343–2389.
20. Chen, G.; Qiu, H.; Prasad, P. N.; Chen, X. Upconversion Nanoparticles: Design, Nanochemistry, and Applications in Theranostics. *Chem. Rev.* **2014**, *114*, 5161–5214.
21. Cheng, L.; Yang, K.; Li, Y.; Chen, J.; Wang, C.; Shao, M.; Lee, S. T.; Liu, Z. Facile Preparation of Multifunctional Upconversion Nanoprobes for Multimodal Imaging and Dual-Targeted Photothermal Therapy. *Angew. Chem., Int. Ed.* **2011**, *123*, 7523–7528.
22. Zhou, L.; Chen, Z.; Dong, K.; Yin, M.; Ren, J.; Qu, X. DNA-Mediated Construction of Hollow Upconversion Nanoparticles for Protein Harvesting and Near-Infrared Light Triggered Release. *Adv. Mater.* **2014**, *26*, 2424–2430.
23. Li, W.; Wang, J.; Ren, J.; Qu, X. Near-Infrared Upconversion Controls Photocaged Cell Adhesion. *J. Am. Chem. Soc.* **2014**, *136*, 2248–2251.
24. Liu, Q.; Feng, W.; Yang, T.; Yi, T.; Li, F. Upconversion Luminescence Imaging of Cells and Small Animals. *Nat. Protoc.* **2013**, *8*, 2033–2044.
25. Punjabi, A.; Wu, X.; Tokatli-Apollon, A.; El-Rifai, M.; Lee, H.; Zhang, Y.; Wang, C.; Liu, Z.; Chan, E. M.; Duan, C.; *et al*. Amplifying the Red-Emission of Upconverting Nanoparticles for Biocompatible Clinically Used Prodrug-Induced Photodynamic Therapy. *ACS Nano* **2014**, *8*, 10621–10630.
26. Bhirde, A.; Xie, J.; Swierczewska, M.; Chen, X. Nanoparticles for Cell Labeling. *Nanoscale* **2011**, *3*, 142–153.
27. Wang, C.; Cheng, L.; Xu, H.; Liu, Z. Towards Whole-Body Imaging at the Single Cell Level Using Ultra-Sensitive Stem Cell Labeling with Oligo-Arginine Modified Upconversion Nanoparticles. *Biomaterials* **2012**, *33*, 4872–4881.
28. Cheng, L.; Wang, C.; Ma, X.; Wang, Q.; Cheng, Y.; Wang, H.; Li, Y.; Liu, Z. Multifunctional Upconversion Nanoparticles for Dual-Modal Imaging-Guided Stem Cell Therapy under Remote Magnetic Control. *Adv. Funct. Mater.* **2013**, *23*, 272–280.
29. Chen, Q.; Wang, C.; Cheng, L.; He, W.; Cheng, Z.; Liu, Z. Protein Modified Upconversion Nanoparticles for Imaging-Guided Combined Photothermal and Photodynamic Therapy. *Biomaterials* **2014**, *35*, 2915–2923.
30. Wang, X.; Liu, K.; Yang, G.; Cheng, L.; He, L.; Liu, Y.; Li, Y.; Guo, L.; Liu, Z. Near-Infrared Light Triggered Photodynamic Therapy in Combination with Gene Therapy Using Upconversion Nanoparticles for Effective Cancer Cell Killing. *Nanoscale* **2014**, *6*, 9198–9205.
31. Xu, L.; Liu, Y.; Chen, Z.; Li, W.; Liu, Y.; Wang, L.; Ma, L.; Shao, Y.; Zhao, Y.; Chen, C. Morphologically Virus-Like Fullerenol Nanoparticles Act as the Dual-Functional Nanoadjuvant for HIV-1 Vaccine. *Adv. Mater.* **2013**, *25*, 5928–5936.
32. Lanzavecchia, A.; Sallusto, F. Regulation of T Cell Immunity by Dendritic Cells. *Cell* **2001**, *106*, 263–266.
33. De Vries, I. J. M.; Lesterhuis, W. J.; Scharenborg, N. M.; Engelen, L. P.; Ruiter, D. J.; Gerritsen, M.-J. P.; Croockewit, S.; Britten, C. M.; Torensma, R.; Adema, G. J.; *et al*. Maturation of Dendritic Cells Is a Prerequisite for Inducing Immune Responses in Advanced Melanoma Patients. *Clin. Cancer Res.* **2003**, *9*, 5091–5100.
34. Mellman, I.; Steinman, R. M. Dendritic Cells: Specialized and Regulated Antigen Processing Machines. *Cell* **2001**, *106*, 255–258.
35. Brunda, M. J.; Luistro, L.; Warrier, R. R.; Wright, R. B.; Hubbard, B. R.; Murphy, M.; Wolf, S. F.; Gately, M. Antitumor and Antimetastatic Activity of Interleukin 12 against Murine Tumors. *J. Exp. Med.* **1993**, *178*, 1223–1230.
36. Carreno, B. M.; Becker-Hapak, M.; Huang, A.; Chan, M.; Alyasiry, A.; Lie, W.-R.; Aft, R. L.; Cornelius, L. A.; Trinkaus, K. M.; Linette, G. P. IL-12p70-Producing Patient DC Vaccine Elicits Tc1-Polarized Immunity. *J. Clin. Invest.* **2013**, *123*, 3383–3394.
37. Gustafsson, K.; Ingelsten, M.; Bergqvist, L.; Nyström, J.; Andersson, B.; Karlsson-Parra, A. Recruitment and Activation of Natural Killer Cells *in Vitro* by A Human Dendritic Cell Vaccine. *Cancer Res.* **2008**, *68*, 5965–5971.
38. Yukawa, H.; Kagami, Y.; Watanabe, M.; Oishi, K.; Miyamoto, Y.; Okamoto, Y.; Tokeshi, M.; Kaji, N.; Noguchi, H.; Ono, K.; *et al*. Quantum Dots Labeling Using Octa-Arginine Peptides for Imaging of Adipose Tissue-Derived Stem Cells. *Biomaterials* **2010**, *31*, 4094–4103.
39. Kraitchman, D. L.; Tatsumi, M.; Gilson, W. D.; Ishimori, T.; Kedziorek, D.; Walczak, P.; Segars, W. P.; Chen, H. H.; Fritzges, D.; Izbudak, I.; *et al*. Dynamic Imaging of Allogeneic Mesenchymal Stem Cells Trafficking to Myocardial Infarction. *Circulation* **2005**, *112*, 1451–1461.
40. Baumjohann, D.; Hess, A.; Budinsky, L.; Brune, K.; Schuler, G.; Lutz, M. B. *In Vivo* Magnetic Resonance Imaging of Dendritic Cell Migration into the Draining Lymph Nodes of Mice. *Eur. J. Immunol.* **2006**, *36*, 2544–2555.
41. Bashour, K. T.; Gondarenko, A.; Chen, H.; Shen, K.; Liu, X.; Huse, M.; Hone, J. C.; Kam, L. C. CD28 and CD3 Have

Complementary Roles in T-Cell Traction Forces. *Proc. Natl. Acad. Sci. U.S.A.* **2014**, *111*, 2241–2246.
42. Kaech, S. M.; Wherry, E. J.; Ahmed, R. Effector and Memory T-Cell Differentiation: Implications for Vaccine Development. *Nat. Rev. Immunol.* **2002**, *2*, 251–262.
43. Migueles, S. A.; Laborico, A. C.; Shupert, W. L.; Sabbaghian, M. S.; Rabin, R.; Hallahan, C. W.; Van Baarle, D.; Kostense, S.; Miedema, F.; McLaughlin, M.; *et al*. HIV-Specific $CD8^+$ T Cell Proliferation Is Coupled to Perforin Expression and Is Maintained in Nonprogressors. *Nat. Immunol.* **2002**, *3*, 1061–1068.
44. Hogquist, K. A.; Jameson, S. C.; Heath, W. R.; Howard, J. L.; Bevan, M. J.; Carbone, F. R. T Cell Receptor Antagonist Peptides Induce Positive Selection. *Cell* **1994**, *76*, 17–27.
45. Seder, R. A.; Darrah, P. A.; Roederer, M. T-Cell Quality in Memory and Protection: Implications for Vaccine Design. *Nat. Rev. Immunol.* **2008**, *8*, 247–258.
46. Dranoff, G. Cytokines in Cancer Pathogenesis and Cancer Therapy. *Nat. Rev. Cancer* **2004**, *4*, 11–22.
47. Tao, Y.; Ju, E.; Li, Z.; Ren, J.; Qu, X. Engineered CpG-Antigen Conjugates Protected Gold Nanoclusters as Smart Self-Vaccines for Enhanced Immune Response and Cell Imaging. *Adv. Funct. Mater.* **2014**, *24*, 1004–1010.
48. Fung-Leung, W.-P.; Schilham, M. W.; Rahemtulla, A.; Kündig, T. M.; Vollenweider, M.; Potter, J.; van Ewijk, W.; Mak, T. W. CD8 Is Needed for Development of Cytotoxic T But Not Helper T Cells. *Cell* **1991**, *65*, 443–449.
49. Harari, A.; Petitpierre, S.; Vallelian, F.; Pantaleo, G. Skewed Representation of Functionally Distinct Populations of Virus-Specific CD4 T Cells in HIV-1-Infected Subjects with Progressive Disease: Changes after Antiretroviral Therapy. *Blood* **2004**, *103*, 966–972.
50. Brossart, P.; Wirths, S.; Stuhler, G.; Reichardt, V. L.; Kanz, L.; Brugger, W. Induction of Cytotoxic T-Lymphocyte Responses *in Vivo* after Vaccinations with Peptide-Pulsed Dendritic Cells. *Blood* **2000**, *96*, 3102–3108.
51. Li, C.; Liang, S.; Zhang, C.; Liu, Y.; Yang, M.; Zhang, J.; Zhi, X.; Pan, F.; Cui, D. Allogenic Dendritic Cell and Tumor Cell Fused Vaccine for Targeted Imaging and Enhanced Immunotherapeutic Efficacy of Gastric Cancer. *Biomaterials* **2015**, *54*, 177–187.
52. Celluzzi, C. M.; Mayordomo, J. I.; Storkus, W. J.; Lotze, M. T.; Falo, L. Peptide-Pulsed Dendritic Cells Induce Antigen-Specific CTL-Mediated Protective Tumor Immunity. *J. Exp. Med.* **1996**, *183*, 283–287.
53. Cheng, L.; Yang, K.; Shao, M.; Lu, X.; Liu, Z. *In Vivo* Pharmacokinetics, Long-Term Biodistribution and Toxicology Study of Functionalized Upconversion Nanoparticles in Mice. *Nanomedicine* **2011**, *6*, 1327–1340.